Reversible and Fast Association Equilibria of a Molecular Chaperone, gp57A, of Bacteriophage T4

Said A. Ali,* Noriyuki Iwabuchi,* Takuro Matsui,* Ken Hirota,† Shun-ichi Kidokoro,†‡§ Munehito Arai,¶‖ Kunihiro Kuwajima,‖ Peter Schuck,** and Fumio Arisaka*

*Graduate School of Bioscience and Biotechnology, Tokyo Institute of Technology, Yokohama, Japan; †Department of Bioengineering, Nagaoka University of Technology, Nagaoka, Niigata, Japan; ‡Precision and Intelligence Laboratory, Tokyo Institute of Technology, Yokohama, Japan; §Genome Science Center, RIKEN, Yokohama, Japan; ¶Institute for Biological Resources and Functions, National Institute of Advanced Industrial Science and Technology, Ibaraki, Japan; ‖Graduate School of Science, University of Tokyo, Tokyo, Japan; and **Division of Bioengineering and Physical Science, ORS, National Institutes of Health, Bethesda, Maryland

ABSTRACT The association of a molecular chaperone, gp57A, of bacteriophage T4, which facilitates formation of the long and short tail fibers, was investigated by analytical ultracentrifugation, differential scanning microcalorimetry, and stopped-flow circular dichroism (CD) to establish the association scheme of the protein. Gp57A is an oligomeric α-helix protein with 79 amino acids. Analysis of the sedimentation velocity data by direct boundary modeling with Lamm equation solutions together with a more detailed boundary analysis incorporating association schemes led us to conclude that at least three oligomeric species of gp57A are in reversible and fast association equilibria and that a 3_{mer}-6_{mer}-12_{mer} model described the data best. On the other hand, differential scanning microcalorimetry revealed a highly reversible two-step transition of dissociation/denaturation, both of which accompanied decrease in CD at 222 nm. The melting curve analysis revealed that it is consistent with a 6_{mer}-3_{mer}-1_{mer} model. The refolding/association kinetics of gp57A measured by stopped-flow CD was consistent with the interpretation that the bimolecular reaction from trimer to hexamer was preceded by a fast α-helix formation in the dead-time. Trimer or hexamer is likely the functional oligomeric state of gp57A.

INTRODUCTION

There are a number of gene products of phage T4, which are essential for the assembly, but are not incorporated into the mature virion. Gp57A is one of them, which facilitates the long and short tail fiber formation (Dickson, 1973). The long tail fibers, encoded by genes 34–37 (King and Laemmli, 1971; Wood and Bishop, 1973; Bishop et al., 1974; Wood et al., 1994), are the sensor for the host bacterial cell, that attach reversibly to the glucose residues on the outer core of lipopolysaccharide on the outer membrane in the case of BE strains (Prehm et al., 1976a) and to OmpC in the case of K-12 strains (Mutoh et al., 1978; Henning and Jann, 1979). After the conformational change of the baseplate, which is triggered by the signal from the long tail fibers via gp9, another baseplate component, the short tail fibers encoded by gene 12 (Kells and Haselkorn, 1974; Mason and Haselkorn, 1972) that had been retracted beneath the baseplate are ejected and irreversibly bind to the heptose part of the inner core of lipopolysaccharide (Riede, 1987). The conformational change of the baseplate induces the sheath contraction and, concomitantly, the tail tube protrudes from the bottom of the baseplate and penetrates into the outer membrane. After the tail tube reaches the inner membrane with the aid of the tail lysozyme, gp5, the injection of the phage genomic DNA into the host cell through the tail tube follows (Simon and Anderson, 1967). A partial high resolution structure of trimeric gp12 that includes the C-terminal head and part of the long shaft has been reported (van Raaij et al., 2001). The shaft part contains a beta-spiral and a short triple-stranded α-helix.

Gp57A is a small protein, containing 79 amino acid residues with the molecular weight of 8,613, where the N-terminal Met is removed. It has an unusual amino acid composition in that it neither contains the aromatic amino acids Trp, Tyr, and Phe nor has His, Pro, and Cys. More than 90% of the polypeptide assumes α-helix based on the far ultraviolet circular dichroism (CD) spectrum (Matsui et al., 1997). Previous studies indicated that the functionally essential part of gp57A resides in the N-terminal region (Hashemolhosseini et al., 1996). It was later shown that gp57A facilitates folding of gp12 in vitro (Burda and Miller, 1999). On the other hand, a temperature-sensitive bypass-mutant of *Escherichia coli* was isolated which does not require gp57A for phage growth, indicating that there is some *E. coli* co-chaperone for the full function of gp57A (Revel et al., 1976).

Gp57A exhibits a highly reversible dissociation and denaturation by heat and denaturing reagents such as urea and guanidine hydrochloride (Gdn-HCl). This high reversibility prompted us to undertake an investigation of the detailed association equilibrium of gp57A. Previously, two of the present authors and co-workers have reported that gp57A is a tetramer (Matsui et al., 1997). This conclusion was based on the weight-average molecular weight which was measured in a limited range of concentrations. However, further studies indicated that the weight-average molecular weight is temperature dependent and the protein is actually in

Submitted April 27, 2003, and accepted for publication May 30, 2003.

Address reprint requests to Fumio Arisaka, PhD, Graduate School of Bioscience and Biotechnology, Tokyo Institute of Technology, 4259 Nagatsuta, Midori-ku, Yokohama 226-8501, Japan. Tel./Fax: 81-45-924-5713; E-mail: farisaka@bio.titech.ac.jp.

0006-3495/03/10/2606/13 $2.00

equilibrium between different oligomeric species. The identification of the oligomeric species was difficult due to the fact that the protein tends to associate to higher molecular weight oligomers at higher protein concentrations.

In the present study, the association equilibrium of gp57A was studied by analytical ultracentrifugation (AUC) to establish the stoichiometry and the scheme of oligomerization. Both sedimentation equilibrium and sedimentation velocity experiments were carried out. The velocity data were analyzed by direct modeling of the sedimentation boundary by finite element solutions of the Lamm equation, using two independent approaches. First, a distribution function of species with different sedimentation coefficients, $c(s)$ (Schuck, 2000; Schuck et al., 2002), was determined. Although this method provides only an apparent sedimentation coefficient distribution for proteins with rapid reversible self-association kinetics, it deconvolutes the effects of diffusion and allows assessment of the heterogeneity of the protein populations and the precise determination of the isotherm of weight-average sedimentation coefficients (Schuck, 2003). Second, solutions of the Lamm equations incorporating specific self-association models were fitted to the data (Schuck, 2003, 1998). Combination of both approaches resulted in a self-association model that is consistent with the observed hydrodynamic behavior of gp57A as well as the thermal-dissociation/denaturation observed by differential scanning micro-calorimetry (DSC) and the refolding/association kinetics observed by stopped-flow circular dichroism (CD). The resultant model of association equilibrium and its implication are discussed.

MATERIALS AND METHODS

Bacteria and plasmid

Plasmid pTB5 contains gene 57A in pT7-5, which expresses genes under T7 promoter. The plasmid was transformed into *E. coli* BL21 (DE3), which carries T7 RNA polymerase on λDE3 integrated into the chromosome of BL21 (Studier and Moffatt, 1986).

Protein expression and purification

Luria broth was used to grow *E. coli*. Luria broth medium contained 10 g Bacto Tryptone, 5 g yeast extract (Difco, Detroit, MI), and 10 g NaCl per liter of distilled water. Buffers A and B were used to purify gp57A. Buffer A is 100 mM Tris, adjusted with HCl to pH 8.0 and buffer B has the same composition as buffer A and supplemented with 100 mM NaCl. Overexpression and purification of gp57A was done as previously described (Matsui et al., 1997).

Analytical ultracentrifugation

Sedimentation velocity and equilibrium experiments were conducted with an Optima XLI (Beckman-Couter, Fullerton, CA), using a 4-hole An60Ti rotor at 20°C (unless noted otherwise). Protein was brought into the experimental buffers (100 mM Tris-HCl, 50 mM NaCl, at pH 8.0, unless otherwise noted) by dialysis, and the dialysate was used as an optical reference. Because gp57A does not possess any aromatic amino acids, the concentration profiles were monitored by their peptide backbone absorbance, using wavelengths of 230–235 nm, and 12-mm or 3-mm pathlength centerpieces, dependent on loading concentration. The extinction coefficient at 230 and 235 nm were determined to be 16,518 and 7633 M^{-1} cm^{-1}, respectively, using BCA protein assay protocol by Pierce Chemical (Rockford, IL) with BSA as a standard. Because of limitations in the wavelength accuracy of the absorption optical detection system in the analytical ultracentrifuge, apparent extinction coefficients were estimated based on the known loading concentration of the protein. Only the sedimentation equilibrium experiments with the highest loading concentrations were observed with the refractometric Rayleigh optics. Sedimentation equilibrium data were acquired at rotor speeds of 12,000, 15,000, and 18,000 rpm, and sedimentation velocity at 50,000 rpm with time intervals of 5 min. The protein partial specific volume ($\bar{v}$) is 0.718 cm^3/g, as determined previously (Matsui et al., 1997), and buffer densities and viscosities were calculated from composition, using the software SEDNTERP (kindly provided by Dr. J. Philo). Sedimentation equilibrium data were edited with the program xlaedit5, to remove data points of the raw XLA data file which are apparently not signals but noise, and and with larger absorption than 1.5. The program MWAVCALC3 is then used to calculate the signal-average buoyant molar mass from a linear plot of the natural logarithm of the absorbance as a function of the square of the radius. By selecting the region which appears a straight line, a best-fit straight line is drawn through that region, and the average concentration and calculated best-fit average buoyant molar mass are displayed. Both programs are kindly provided by Dr. A. Minton. The isotherm of buoyant molar mass $M_b(c)$ was fitted to 3_{mer}-6_{mer}-12_{mer} model using the software f_mw8 (kindly provided by Dr. A. Minton).

Hydrodynamic modeling of the sedimentation velocity data

Sedimentation velocity analysis was based on direct modeling of the sedimentation boundary, using finite-element solutions of the Lamm equation

$$\frac{\partial \chi}{\partial t} = \frac{1}{r}\frac{\partial}{\partial r}\left[rD\frac{\partial \chi}{\partial r} - s\omega^2 r^2 \chi\right], \tag{1}$$

where $\chi(r, t)$ describes the evolution of the spatial concentration distribution of a single sedimenting species in the centrifugal field, with r denoting the distance from the center of rotation, ω the rotor angular velocity, and s and D the macromolecular sedimentation and diffusion coefficient, respectively (Schuck, 1998; Lamm, 1929). For the sedimentation coefficient distribution $c(s)$, the data were modeled as a superposition of solutions to Eq. 1,

$$a(r,t) \cong \int_{s_{min}}^{s_{max}} c(s)\chi(s, D(s), r, t)ds, \tag{2}$$

which was calculated with maximum entropy regularization, as implemented in the software SEDFIT (www.analyticalultracentrifugation.com) and described previously (Schuck, 2000). A confidence level of 0.95 was used to scale the regularization. The analysis was combined with algebraic decomposition of the systematic time-invariant noise (Schuck and Delemer, 1999), and the meniscus position and the weight-average frictional ratio f/f_0 were optimized in a nonlinear regression (Schuck et al., 2002; Dam and Schuck, 2003).

For the sedimentation analysis with different explicit self-association schemes, the Lamm equation was solved with locally concentration-dependent sedimentation and diffusion coefficients

$$\frac{\partial \chi}{\partial t} = \frac{1}{r}\frac{\partial}{\partial r}\left[rD(\chi)\frac{\partial \chi}{\partial r} - s(\chi)\omega^2 r^2 \chi\right], \tag{3}$$

where $s(\chi)$ and $D(\chi)$ are the isotherms of the weight-average sedimentation coefficient and the gradient-average diffusion coefficient as a function of

total local protein concentration, respectively (Schuck, 1998; Cox, 1969). These are standard isotherms calculated based on mass action and mass conservation laws for different self-association schemes, and their use for the sedimentation analysis assumes that self-association is fast on the timescale of sedimentation. Several sedimentation velocity data sets obtained at different loading concentration were modeled globally with the software SEDPHAT (www.analyticalultracentrifugation.com) as described in Schuck (2003), using the monomer and oligomer *s*-values and the binding constants as global parameters, and meniscus position, concentrations, and time-invariant noise as local parameters for each experiment.

Differential scanning calorimetry

The apparent heat capacity was evaluated using the first scanning data of the sample solution and the data of buffer solution just before and after the sample scanning by differential scanning calorimeter, MCS-DSC and VP-DSC (MicroCal, Studio City, CA). The 50 mM sodium phosphate was used for the buffer at pH 7.5 and 8.0, and 20 mM glycine/HCl buffer was used at pH 2.8. The protein stock solution was dialyzed extensively against a large volume of buffer solution. The concentration of the stock solution after the dialysis was evaluated by the absorbance as mentioned above and the sample solution at various protein concentrations was prepared by mixing the stock solution and the dialyzed buffer solution. The scanning rate was 1 K/min for all the measurements except for the scan to check the scanning rate dependence of the transition. The apparent heat capacity obtained by 0.5-K/min scanning rate was found to agree completely with that by 1-K/min at all the pH conditions studied in this article. The reversibility was also checked by the second scanning of the sample solution at all conditions and the peak of the second scanning was almost the same as the first scanning.

The two-state analysis and double deconvolution method for the system with self-dissociation/association process (Kidokoro et al., 1988) were applied to the apparent heat capacity function with the assumption that the heat capacity functions of native and denatured state were described as the linear function of temperature. The rough values for the thermodynamic parameters of the transition were obtained by these methods. The nonlinear least-squares method was used to refine the parameters as described previously (Kidokoro et al., 1988). The global fitting to determine the common thermodynamic parameters among the various protein concentrations at the same pH was developed to determine the model and thermodynamic parameters finally. The apparent Gibbs free energy change from i^{th} state to j^{th} state at various protein concentrations M, $\Delta G_{ij}^{\text{app}}(T, M)$ was described as

$$\Delta G_{ij}^{\text{app}}(T, M) = \Delta G_{ij}^{0}(T, M_0) + RT(m_j - m_i)\ln(M/M_0), \quad (4)$$

where $\Delta G_{ij}^{0}(T, M_0)$ is the standard Gibbs free energy change at the standard concentration, M_0; m_i and m_j are the stoichiometry coefficients of i^{th} and j^{th} state, respectively; R is the gas constant; and T is absolute temperature. By this relationship, the Gibbs free energy change at each protein concentration was calculated using the common standard Gibbs free energy change whose thermodynamic parameters were adjusted to fit the data in the global fitting method. The standard Gibbs free energy change, $\Delta G_{ij}^{0}(T, M_0)$, was the function of temperature and was described in the following equation in principle as discussed previously (Kidokoro et al, 1988),

$$\Delta G_{ij}^{0}(T, M_0) = -\Delta a_{ij} T(T - T_{m,ij}) - \Delta b_{ij} T \ln(T/T_{m,ij}) + \Delta c_{ij}(1 - T/T_{m,ij}), \quad (5)$$

where $T_{m,ij}$ is the midpoint temperature of the thermal transition between i^{th} and j^{th} state, and Δa_{ij}, Δb_{ij}, and Δc_{ij} are the fitting parameters to determine the enthalpy function of temperature as shown in Eq. 6:

$$\Delta H_{ij}(T) = \Delta a_{ij} T^2 + \Delta b_{ij} T + \Delta c_{ij}. \quad (6)$$

To decrease the dependency among the parameters and to decrease the estimation error for the parameters, two fitting parameters, $\Delta C_{p,ij}(T_{m,ij})$ and $\Delta H_{ij}(T_{m,ij})$, are used in practice as the fitting parameters instead of the two parameters, Δb_{ij} and Δc_{ij}, which have the following relationships to other parameters, respectively.

$$\Delta b_{ij} = -2\Delta a_{ij} T_{m,ij} + \Delta C_{p,ij}(T_{m,ij}), \quad (7)$$

$$\Delta c_{ij} = \Delta a_{ij} T_{m,ij}^2 - \Delta C_{p,ij}(T_{m,ij}) T_{m,ij} + \Delta H_{ij}(T_{m,ij}). \quad (8)$$

$\Delta C_{p,ij}(T_{m,ij})$ and $\Delta H_{ij}(T_{m,ij})$ are the heat capacity change and enthalpy change between i^{th} and j^{th} states at the transition temperature.

In this method, the statistical weight of the molar heat capacity was set to be proportional to the protein concentration where the heat capacity function was obtained because the signal-to-noise ratio was normally expected to be proportional to the protein concentration in DSC measurement. The program for this global fitting was written in FORTRAN and used the nonlinear least-squares method program package, SALS (Nakagawa and Oyanagi, 1980).

CD and secondary structure estimation

The far-UV CD spectrum of gp57A, pre-equilibrated with pH 8.0, 50 mM sodium phosphate buffer, between 190 and 240 nm, was measured as a function of temperature on a J-720 spectropolarimeter (JASCO, Tokyo, Japan) in a 1-mm pathlength cell. The spectrum at different peptide concentrations were used to estimate the secondary structure by CONTIN (Provencher and Glockner, 1981).

Kinetic refolding measurement

Kinetic refolding/association measurements were carried out on a Jasco J-720 spectropolarimeter. The stopped-flow apparatus attached to the spectropolarimeter was specially designed and constructed by Unisoku (Hirakata, Osaka, Japan). (Kuwajima et al., 1987; Arai and Kuwajima, 1996). The pathlength of the cuvette was 1 mm, and the dead-time was 15 ms. The refolding reaction was initiated by a Gdn-HCl concentration jump from 2.6 to 0.23 M. Final protein concentration was 0.0085 ~0.085 mg/ml (0.987 ~9.87 μM in a monomer concentration). The solutions contained 0.1 M sodium phosphate (pH 8.0). The experiments were performed at 20°C.

The kinetic refolding curves of gp57A were analyzed assuming the bimolecular, trimolecular, and tetramolecular reactions and were fit to the following equations:

1. A bimolecular reaction ($2A \rightarrow B$):

$$\theta_{\text{obs}} = \theta_B + \frac{(\theta_A - \theta_B)}{1 + k_{\text{app}} t}; \quad (9)$$

2. A trimolecular reaction ($3A \rightarrow B$):

$$\theta_{\text{obs}} = \theta_B + \frac{(\theta_A - \theta_B)}{(1 + k_{\text{app}} t)^{1/2}}; \quad (10)$$

3. A tetramolecular reaction ($4A \rightarrow B$):

$$\theta_{\text{obs}} = \theta_B + \frac{(\theta_A - \theta_B)}{(1 + k_{\text{app}} t)^{1/3}}, \quad (11)$$

where θ_{obs} is the observed ellipticity; θ_A and θ_B are the ellipticities of the species A and B, respectively; and k_{app} is the apparent rate constant of the reaction (Steinfeld et al., 1989; Milla and Sauer, 1994). k_{app} (s^{-1}) for the bimolecular reaction corresponds to $2A_0 k_f$, where A_0 (M) is the initial concentration of the species A, and k_f ($M^{-1}\ s^{-1}$) is the actual second-order rate constant of the $2A \rightarrow B$ reaction.

RESULTS

Concentration dependence of the weight average buoyant molecular weight of gp57A

The weight average buoyant molecular weight, $M(1 - \bar{\nu}\rho)$ or M_b, of gp57A was measured at a concentration range between 0.02 mg/ml and 7 mg/ml to characterize the association equilibrium. In Fig. 1, M_b is plotted against the logarithm of the protein concentration. The buoyant molecular weight of monomeric gp57A is 2429. Except for a number of data points at the lowest buoyant molecular weights, the M_b increases from ~10,000 up to 30,000 as the concentration increases, which corresponds to tetramer and dodecamer. The molecular weight appears to increase further when the concentration is further increased. In this situation, it is not simple to determine the association scheme by curve-fitting to the M_b isotherm. The solid line in the graph is calculated according to the 3_{mer}-6_{mer}-12_{mer} model using a software, f_mw8, kindly provided by A. Minton, but other models, such as 4_{mer}-8_{mer}-16_{mer}, also fit reasonably well (data not shown), and it was not possible to unambiguously choose one best-fit model. However, when the 3_{mer}-6_{mer}-12_{mer} model was used to fit the data, the obtained values for K_{3-6} and K_{6-12} coincided with those obtained from the sedimentation velocity analysis in the next section within experimental errors.

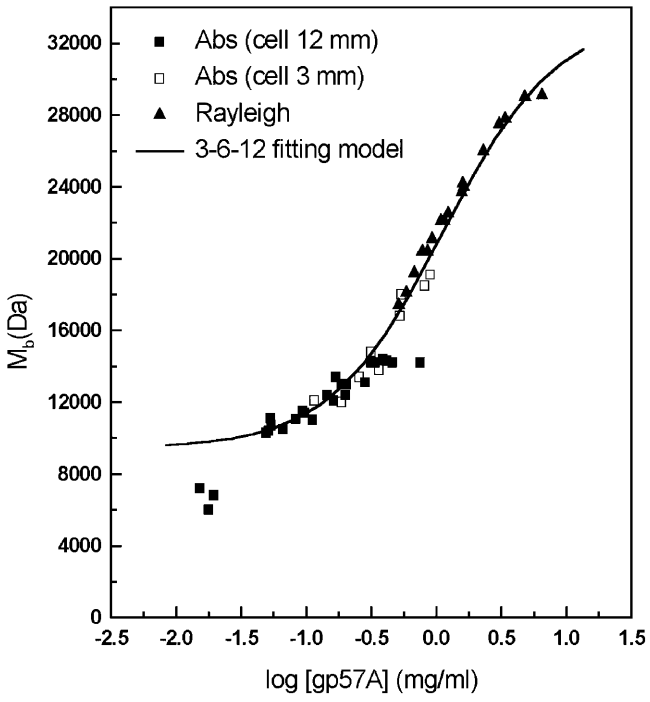

FIGURE 1 Dependence of the weight average buoyant molar mass (M_b) upon the weight concentration of gp57A, determined from sedimentation equilibrium experiments using a range of loading concentrations from 0.02 to 7.0 mg/ml, at 20°C at rotor speeds of 12,000, 15,000, and 18,000 rpm. Absorbance and Rayleigh optics as well as different optical pathlength centerpieces are used to cover the whole range of concentration as indicated by the different symbols, and at each concentration global modeling was used to calculate the best-fit buoyant molar mass. The whole data sets are globally fitted to the trimer-hexamer-dodecamer model (*solid line*). The binding constants, K_{3-6} and K_{6-12}, are $(2.17 \pm 0.10) \times 10^4\ M^{-1}$ and $(2.63 \pm 0.10) \times 10^4\ M^{-1}$, respectively.

Analysis of the association scheme by sedimentation velocity

Sedimentation velocity experiments were carried out at a number of loading concentrations in the range from 0.1 to 2.1 mg/ml, and the data were analyzed first by modeling the sedimentation boundaries as superpositions of finite element solutions of the Lamm equation for noninteractions species. The obtained distribution functions of sedimentation coefficients, $c(s)$, are shown for each loading concentration as indicated in Fig. 2. There are several peaks, indicating the existence of multiple oligomeric species. However, it is noted that the peaks of $c(s)$ are broader than those expected for discrete noninteracting components and the apparent peak sedimentation coefficients are highly concentration-dependent, shifting the s-values to higher values at higher loading concentrations. This indicated that the boundaries are ''reaction boundaries,'' in which the sedimenting species interconvert on the timescale of sedimentation or faster, and

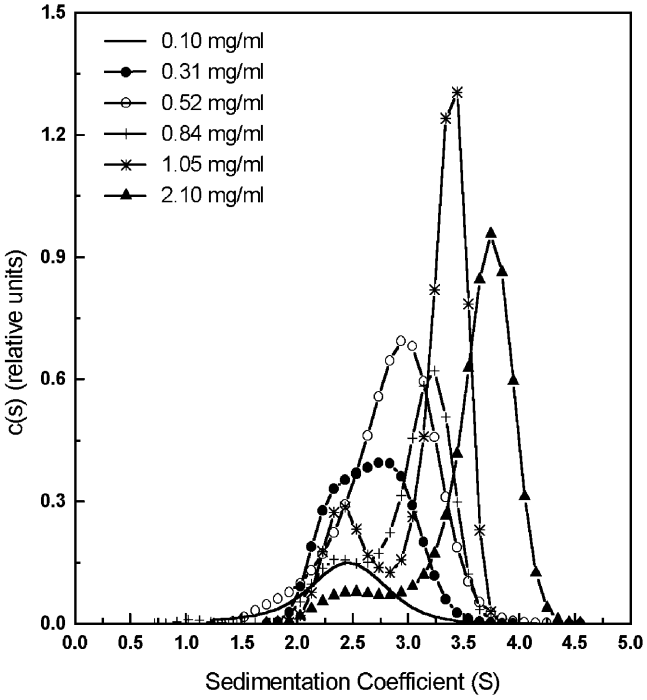

FIGURE 2 Sedimentation coefficient distribution $c(s)$ derived from sedimentation velocity data at 50,000 rpm and 20°C. Loading concentrations were 0.1, 0.31, 0.52, 0.84, 1.05, and 2.1 mg/ml. The $c(s)$ distribution was derived with the frictional ratio (f/f_0) and the base line offset as a floating parameters, and with maximum entropy regularization with a confidence limit of $p = 0.95$.

as a consequence the observed peaks do not correspond to any particular individual oligomeric species but instead reflect some weight-average of the sedimenting species. All the velocity data at different loading concentrations are then globally fitted to finite element Lamm equation solutions that incorporate explicitly different models for the self-association scheme (Schuck, 2003, 1998). First, two-state models, 2_{mer}-6_{mer}, 3_{mer}-6_{mer}, and 4_{mer}-8_{mer}, were tested, but no satisfactory results were obtained. The values for the sum of squared deviations (SOSQ) for these models were 4.028, 3.686, and 3.567, respectively. We then proceeded to fit the data to three-state models, 2_{mer}-6_{mer}-12_{mer}, 3_{mer}-6_{mer}-12_{mer}, and 4_{mer}-8_{mer}-16_{mer}. The SOSQ values for these models were 3.492, 3.511, and 3.562, respectively. We may statistically exclude any model with a SOSQ value larger than 3.521 with 95.4% confidence. The 4_{mer}-8_{mer}-16_{mer} model is thus excluded. The remaining two models, 2_{mer}-6_{mer}-12_{mer} and 3_{mer}-6_{mer}-12_{mer}, both fit the data reasonably well. However, from the following criteria, the 3_{mer}-6_{mer}-12_{mer} model was unambiguously selected. The best-fit sedimentation coefficients, frictional ratios (f/f_0), and axial ratios (a/b) of the hydrodynamically equivalent prolate ellipsoid for the different oligomers are listed in Table 1. The frictional ratios f/f_0 and the axial ratios a/b are calculated where 0.3 g/g estimate for hydration is included. It should be noted that the axial ratios of the hydrodynamically equivalent prolate ellipsoids are a measure of the compactness or shape asymmetry of the protein, but may not represent well the actual shape of the protein. For the 3_{mer}-6_{mer}-12_{mer} model, all the s-, f/f_0-, and a/b-values appear reasonable. On the other hand, for the 2_{mer}-6_{mer}-12_{mer} model, the best-fit value for s_2 is larger than the possible sedimentation coefficient of a hydrated molecule in the most compact spherical form, and accordingly f/f_0 for the dimer is unphysically small for a hydrated molecule. On the other hand, s_6 is too small and f/f_0 value is too large, corresponding to an unreasonably extended hexamer. We, therefore, concluded that the 3_{mer}-6_{mer}-12_{mer} model is the right one. A subset of sedimentation velocity data and the boundary fits leading to this model is shown in Fig. 3.

pH dependence of the association equilibrium

The association equilibrium of gp57A is highly dependent on pH. Lower pH favors association (Fig. 4). At pH 9.0, only one peak with a sedimentation coefficient of 2.6 S is present, which suggests the presence of mixtures of rapidly interconverting trimers and hexamers. In a boundary model with explicit incorporation of the 3_{mer}-6_{mer}-12_{mer} model, the 12_{mer} concentration was below the detection limit. As the pH values are lowered, two reaction boundaries appear and the peak values shifted toward higher sedimentation coefficients. At pH 3.8, which is close to the isoelectric point of 4.2, the protein precipitated and it was not possible to measure the association equilibrium (data not shown). At pH 2.8, a sharp peak with the s-value of 1.7 S which is lower than that of the trimer determined at pH 8.0 appeared, indicating either the presence of a trimer with more extended conformation, or the partial dissociation into monomers. This is confirmed by a Lamm equation model with explicit self-association, which did not model the data well with oligomeric species of the s-values previously determined at pH 8.0, but modeled the data well as a single trimeric species with a small degree of dissociation. Weight average sedimentation coefficients, s_w, are plotted against pH in the inset of Fig. 4.

Temperature dependence of association of gp57A

The temperature dependence of association of gp57A was studied by sedimentation velocity at a number of temperatures between 4 and 37°C at pH 8.0. The resultant $c(s)$ curves obtained by SEDFIT are shown in Fig. 5 *a*. At low temperatures, 4 and 12°C, the association equilibrium is shifted to higher association species. At higher temperatures, the species with higher sedimentation coefficients decreased, which increased the trimer and hexamer concentrations. At 37°C, dodecamer virtually disappeared and some fraction of the trimer appeared to dissociate further into monomers. Measurements of sedimentation velocity were carried out at three loading concentrations, 0.42, 0.52, and 0.63 mg/ml, and the data were fitted the Lamm equation to 3_{mer}-6_{mer}-12_{mer} model, using the s-value of each oligomer as determined above. The observed temperature dependence of the trimer-hexamer and the hexamer-dodecamer association constant is shown as the van't Hoff plot in Fig. 5 *b*. Again, we found that lower temperature favors the association of trimers to hexamers, whereas the formation of dodecamer appeared relatively constant or slightly decreasing with lower temperature.

TABLE 1

3_{mer}-6_{mer}-12_{mer}			2_{mer}-6_{mer}-12_{mer}		
$s_3 = 2.16$ S	$s_6 = 3.25$ S	$s_{12} = 4.59$ S	$s_2 = 2.3$ S	$s_6 = 2.71$ S	$s_{12} = 5.05$ S
$f/f_0 = 1.53$	$f/f_0 = 1.61$	$f/f_0 = 1.81$	$f/f_0 = 1.10$	$f/f_0 = 1.93$	$f/f_0 = 1.64$
$a/b = 6.7$	$a/b = 8.0$	$a/b = 11.3$	—	$a/b = 13.5$	$a/b = 8.5$

The best-fit sedimentation coefficients (s), frictional ratios (f/f_0), and axial ratios (a/b) of the hydrodynamically equivalent prolate ellipsoid for the different oligomers, including 0.3 g/g as an estimate for hydration.

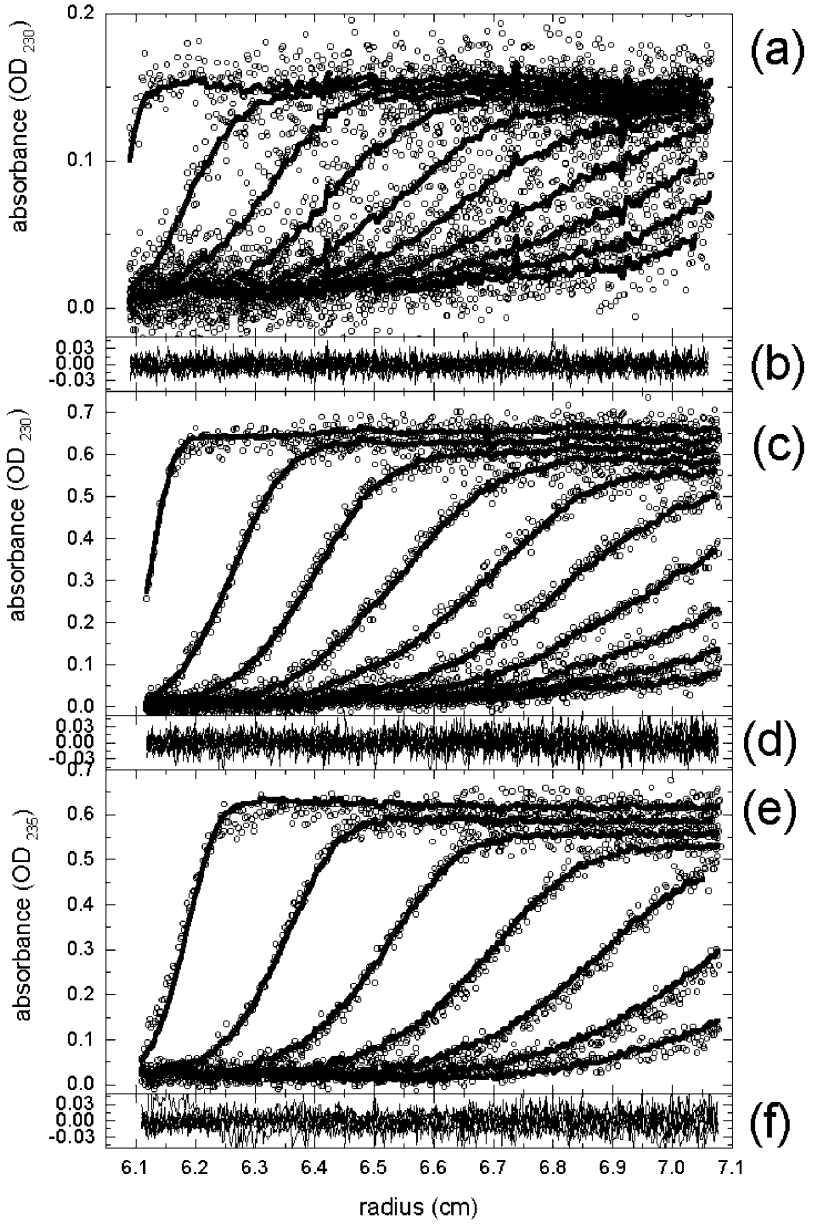

FIGURE 3 Raw sedimentation velocity data and global fit incorporating an explicit trimer-hexamer-dodecamer model. Shown are only every 10th experimental absorbance profile (*circles*) obtained at a rotor speed of 50,000 rpm at 20°C at pH 8.0, at concentrations of 0.1 mg/ml (*a*), 0.52 mg/ml (*c*), and 2.1 mg/ml (*e*). The scans shown are taken from equivalent timepoints for each loading concentration. A global fit with a trimer-hexamer-dodecamer model was achieved with a larger set of sedimentation data at loading concentrations of 0.1, 0.31, 0.52, 1.05, and 2.1 mg/ml which resulted in binding constants of $K_{3\text{–}6} = (3.4 \pm 0.6) \times 10^4\ M^{-1}$ and $K_{6\text{–}12} = (7.62 \pm 1.3) \times 10^3\ M^{-1}$, with sedimentation coefficients $s_3 = 2.16 \pm 0.09$ S, $s_6 = 3.25 \pm 0.04$ S, and $s_{12} = 4.59 \pm 0.08$ S. The solid lines show the best-fit sedimentation distributions (including time-invariant noise components). The residuals of the fits corresponding to the data in *a*, *c*, and *e* are shown in *b*, *d*, and *f*, respectively.

Heat-induced dissociation/denaturation of gp57A as observed by differential scanning microcalorimetry (DSC)

The heat capacity of gp57A as a function of temperature was measured at pH 8.0, 7.5, and 2.8. The heat observed in the reheating scan just after the first scan agreed very well with that in the first scan in all the conditions of this study, showing the good reversibility of the thermal transition (data not shown). The heat obtained in the scanning rate of 0.5 K/min also coincided to that in the 1-K/min scan, indicating the folding/unfolding rate is rapid enough to reach equilibrium at each temperature in the 1-K/min scan (data not shown). The good reversibility and equilibrium at each temperature enable us to analyze the function observed by DSC with well-established thermodynamic method; two-state analysis, double deconvolution, and least-squares fitting with theoretical models.

At the neutral pH, the heat capacity function of gp57A had the two peaks as shown in Fig. 6 (in the case at pH 8.0), indicating the existence of a stable intermediate state, whereas the heat capacity function at pH 2.8 showed only one peak (Fig. 7). It was clear that the shape of all these peaks was unsymmetrical and the heat capacity changed more rapidly in the higher temperature side. When the thermal denaturation accompanies the dissociation process, the heat capacity should possess such a shape. The peak temperature of all the peaks observed in this study clearly increased as the protein concentration increased. This de-

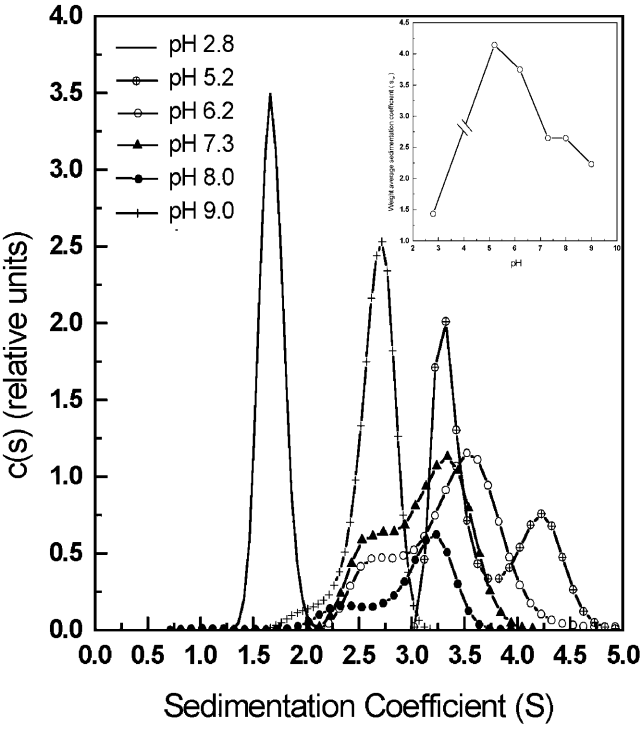

FIGURE 4 The pH dependence of the self-association of gp57A. The protein was dialyzed against buffers at different pH and sedimented at loading concentrations of 0.1, 0.36, 0.63, 1.05, 1.57, and 2.1 mg/ml at a rotor speed of 50,000 rpm and a temperature of 20°C. Shown are the sedimentation coefficient distributions for 0.63 mg/ml at pH values of 2.8, 5.2, 6.2, 7.3, 8.0, and 9.0, respectively. The buffers used are 5 mM NH_4-acetate, 100 mM NaCl at pH 2.8; 100 mM Na-acetate, 50 mM NaCl at pH 5.2; 100 mM MES buffer, 50 mM NaCl at pH 6.2; 100 mM Tris-HCl, 50 mM NaCl at pH 7.3 and pH 8.0; and 100 mM glycine, 50 mM NaCl at pH 9.0, respectively. (*Inset:* s_w vs. pH.)

pendence also indicated that all the thermal transitions of gp57A observed in this study accompanied self-dissociation.

By the double-deconvolution analysis for the system including self-dissociation/association process, the thermodynamic parameters change with the transition; enthalpy change, ΔH, heat capacity change, ΔC_p, and transition temperature, T_m, can be roughly determined with assuming the stoichiometry coefficients for the three thermodynamic states—native, intermediate, and denatured. We assumed that the heat-denatured state of gp57A is monomer so that the coefficient for that state could be assigned to *one* when monomer is used as the unit of molar concentration. All the combinations of the stoichiometry coefficients for native and intermediate states from monomer to decamer were tried to analyze the heat capacity functions at neutral pH. For example, the heat capacity function at pH 8.0, 2.0 mg/ml concentration, could be fitted by the theoretical curves with 4_{mer}-3_{mer}-1_{mer}, 5_{mer}-3_{mer}-1_{mer}, and 6_{mer}-3_{mer}-1_{mer} models for native-intermediate-denatured states from the viewpoint of very small residual deviation of these models. Although only the minimum residual deviation for these data were achieved by the model of 5_{mer}-3_{mer}-1_{mer}, the difference among these

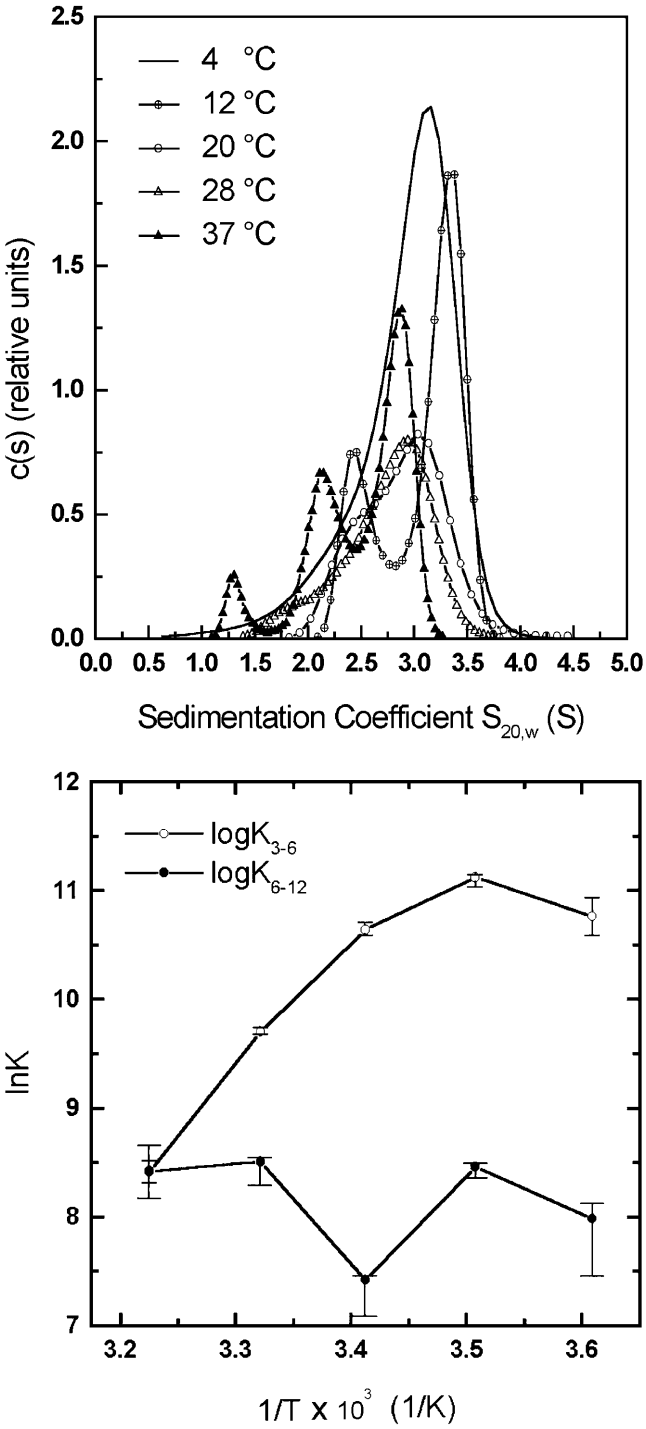

FIGURE 5 (*a*) Temperature dependence of the self-association of gp57A. Sedimentation velocity experiments were conducted at temperatures of 4, 12, 20, 28, and 37°C, at a rotor speed of 50,000 rpm and at pH 8.0. Shown are the sedimentation coefficient distributions $c(s)$ derived from the data at a loading concentration of 0.63 mg/ml. A global analysis using a trimer-hexamer-dodecamer model was globally fitted to the sedimentation data from loading concentrations of 0.42, 0.52, and 0.63 mg/ml, using the predetermined sedimentation coefficients for each oligomer. (*b*) Shows a van't Hoff plot of the temperature dependence of the trimer-hexamer and the hexamer-dodecamer association step.

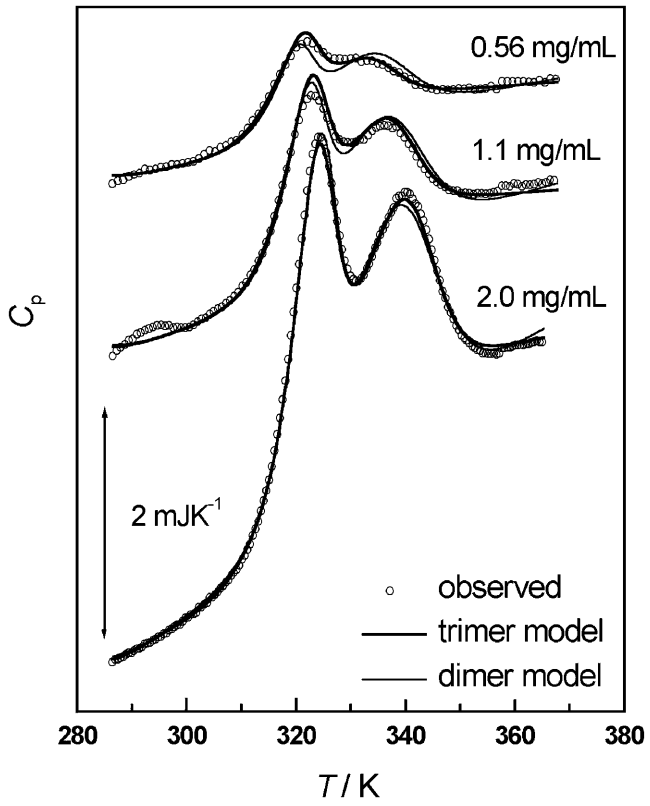

FIGURE 6 Observed heat capacity of gp57A in pH 8.0, 50 mM sodium phosphate buffer with various protein concentration and theoretical functions. Open circles are the observed and the solid lines are the best-fitted functions by global analysis, with the same thermodynamic parameters for all the concentrations, represented by thick lines (trimer intermediate model) and thin lines (dimer intermediate model), respectively. The protein concentrations are indicated in the figure.

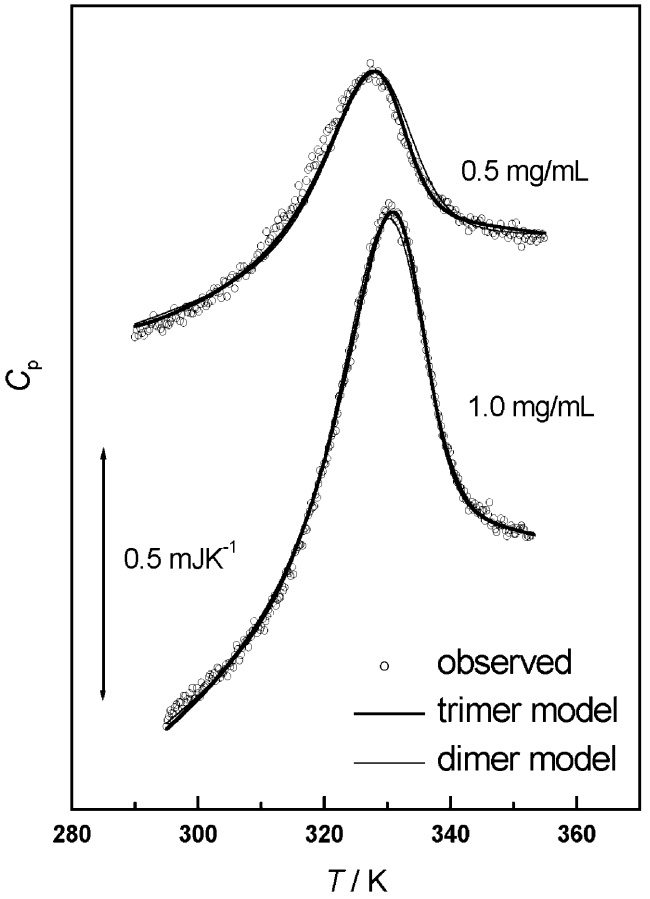

FIGURE 7 Observed heat capacity of gp57A in pH 2.8, 20 mM glycine buffer with different protein concentration and theoretical functions. (Meaning of *symbols* and *lines* are the same as in Fig. 6.)

models were small and it was dangerous to fix the model only from the data of a protein concentration, as discussed previously (Kidokoro et al., 1988).

Generally speaking, the transition temperature should depend on protein concentration more strongly with the large deviation of the stoichiometry coefficients of these two states, which indicates that the concentration dependence of the transition gives additional information to evaluate the stoichiometry coefficient. The global fitting method is efficient to use this kind of information by fitting the data of various protein concentrations at once under the same pH with the same thermodynamic parameter change above mentioned. All the combinations of the stoichiometry coefficients for native and intermediate states are tested for the global fitting and the best-fitted model was found to be 6_{mer}-3_{mer}-1_{mer} with the fixed stoichiometry coefficient for the denatured state. Furthermore, all the stoichiometry coefficients were treated as the fitting parameters in the global fitting, and we calculated their ratios to evaluate the association number for the native and intermediate state. These numbers for native state were 6.0 and 5.6 and those for the intermediate state were 3.0 and 3.0 for the data at pH 8.0 and 7.5, respectively. The concentration dependence of all the peak temperatures in Fig. 6 seemed to be completely explained by the 6_{mer}-3_{mer}-1_{mer} transition model. These results strongly indicate that the thermal transition at neutral pH around these protein concentrations was 3-state transition, with hexamer-native, trimer-intermediate, and monomer-denatured states.

At pH 2.8, the heat capacity function was analyzed by two-state analysis and was found to be explained by the 3_{mer}-1_{mer} two-state model. In this case also, the stoichiometry coefficient of the denatured state was first assumed to be *one* and that of the native state was tested in the range from monomer to decamer. Two models, the 2_{mer}-1_{mer} and 3_{mer}-1_{mer} models, were found to fit the data of 1.0 mg/ml concentration very well and the residual deviations of these models were almost the same. To use the information on concentration dependence even at this pH, the global fitting was applied with various native association numbers from 1–10. Among these models, the 3_{mer}-1_{mer} model was found to have the smallest residual deviation. Finally, all the stoichiometry coefficients were fitted in the analysis, and the association number of the native state, as the ratio of

the coefficients of denatured and native states, was calculated as 3.0. This result indicates that the observed thermal transition at acidic region was the transition from trimer to monomer state.

The thermodynamic parameter changes obtained from the global fitting were summarized in Table 2. At neutral pH, the native and intermediate states are more stable at pH 7.5 than at pH 8.0, judging from the pH dependence of transition temperature. At acidic pH, the hexamer native state is considered to have become too unstable to exist, so that the initial trimer of the acidic condition may be assigned to be the same as the trimer intermediate at neutral pH. Therefore, the thermodynamic parameter change at pH 2.8 is categorized to the transition from intermediate to denatured state in this table.

Heat denaturation as observed by CD

Under the same condition as in Fig. 6, the thermal transition was also monitored by CD at 222 nm (Fig. 8, *a* and *b*). Although the dissociation appears a single transition, the derivative with respective to temperature revealed two peaks corresponding approximately to the same T_m values as in DSC, indicating that both transitions at 324 K and 337 K are accompanied by a decrease in α-helix content.

Measurement of refolding/association kinetics of gp57A by stopped-flow CD

Gp57A was completely denatured in 2.6 M Gdn-HCl and the refolding/ association kinetics was observed by diluting the solution down to 0.23 M of Gdn-HCl. The dead-time of the measurement was 15 ms. The stopped-flow CD data were modeled by three different association models, including a monomer-dimer, monomer-trimer, and monomer-tetramer association (see Materials and Methods). Only the dimerization model could describe the data well (Fig. 9 *a*). The stopped-flow CD measurements were carried out at a concentration range between 0.0085 and 0.085 mg/ml. All the data sets were modeled well by an apparent dimerization or bimolecular reaction scheme and the obtained apparent dimerization rate constants were plotted against the protein concentration (Fig. 9 *b*). The apparent refolding rate was a linear function of the protein concentration, as expected for a bimolecular reaction. Apparently, some decrease in CD at 222 nm with the residue ellipticity of $\sim -7500°$ cm^2 dmol^{-1} had already taken place (Fig. 9 *c*), and the association of 1_{mer} into 3_{mer} has likely already taken place within the dead-time of the stopped-flow experiment. We interpret the bimolecular reaction as the association of 3_{mer} to 6_{mer}, which is consistent with all the other data described above. Furthermore, the fact that almost no change in ellipticity is observed after several seconds suggests that the oligomerization reaction is much faster than the order of time for performing sedimentation velocity experiments, justifying the use of the rapid equilibrium assumption in the direct boundary modeling with the Lamm equation.

TABLE 2

	pH	T_m/K	ΔH/kJ mol^{-1}	ΔC_p/kJK^{-1} mol^{-1}
$\frac{1}{6}N_6 \leftrightarrows \frac{1}{3}I_3$	7.5	324.2	88	2.0
	8.0	323.6	77	2.2
$\frac{1}{6}N_6 \leftrightarrows D$	7.5	329.6	204	3.4
	8.0	327.7	177	3.8
$\frac{1}{3}I_3 \leftrightarrows D$	2.8	328.7	126	0.9
	7.5	334.4	116	1.8
	8.0	331.4	98	1.7

Thermodynamic parameters of thermal transition between the thermodynamic states observed by differential scanning calorimetry with the model of native hexamer, denatured monomer and the trimer intermediate state; $(1/6)N_6 \leftrightarrows (1/3)I_3 \leftrightarrows D$. T_m is the midpoint temperature of the transition where the Gibbs free energy change between the two states becomes zero at the protein concentration, 1.0 mg/ml. ΔH and ΔC_p are the enthalpy and heat capacity difference between the thermodynamic states. In this table, monomer is considered as a unit of mol.

DISCUSSION

Combinations of different physical techniques are extremely useful for fully elucidating the molecular mechanisms of folding and self-association of proteins. In the present study, thermodynamic, kinetic, and hydrodynamic methods were employed to unambiguously determine the reaction scheme of unfolding/dissociation and folding/association of gp57A of bacteriophage T4. The analysis of the sedimentation boundaries observed in analytical ultracentrifugation experiments gave rise to the overall reaction scheme. Changes in thermodynamic functions associated with the folding and oligomerization reactions were directly assessed by the calorimetric technique. The stopped-flow CD in the peptide secondary-structure region enabled us to analyze the kinetics of conformational changes during the reactions, and was particularly useful for gp57A that does not have aromatic residues.

Oligomeric states of gp57A

Gp57A which facilitates formation of the long and short tail fibers is a unique protein in its highly reversible dissociation/ unfolding property and the unusual amino acid composition, where no Trp, Tyr, Phe, His, Cys, or Pro is present. The determination of the association scheme is usually not so complicated if the upper limit of the oligomeric state is clearly defined. However, some proteins such as tubulin tend to associate higher and higher oligomeric states at higher concentration, and in this situation determination of the association scheme is not simple (Rivas et al., 1999). Gp57A is such a protein. We have carried out sedimentation equilibrium, light scattering, chemical crosslinking, and mass spectrometry to resolve the association scheme without success (data not shown). It was the sedimentation velocity

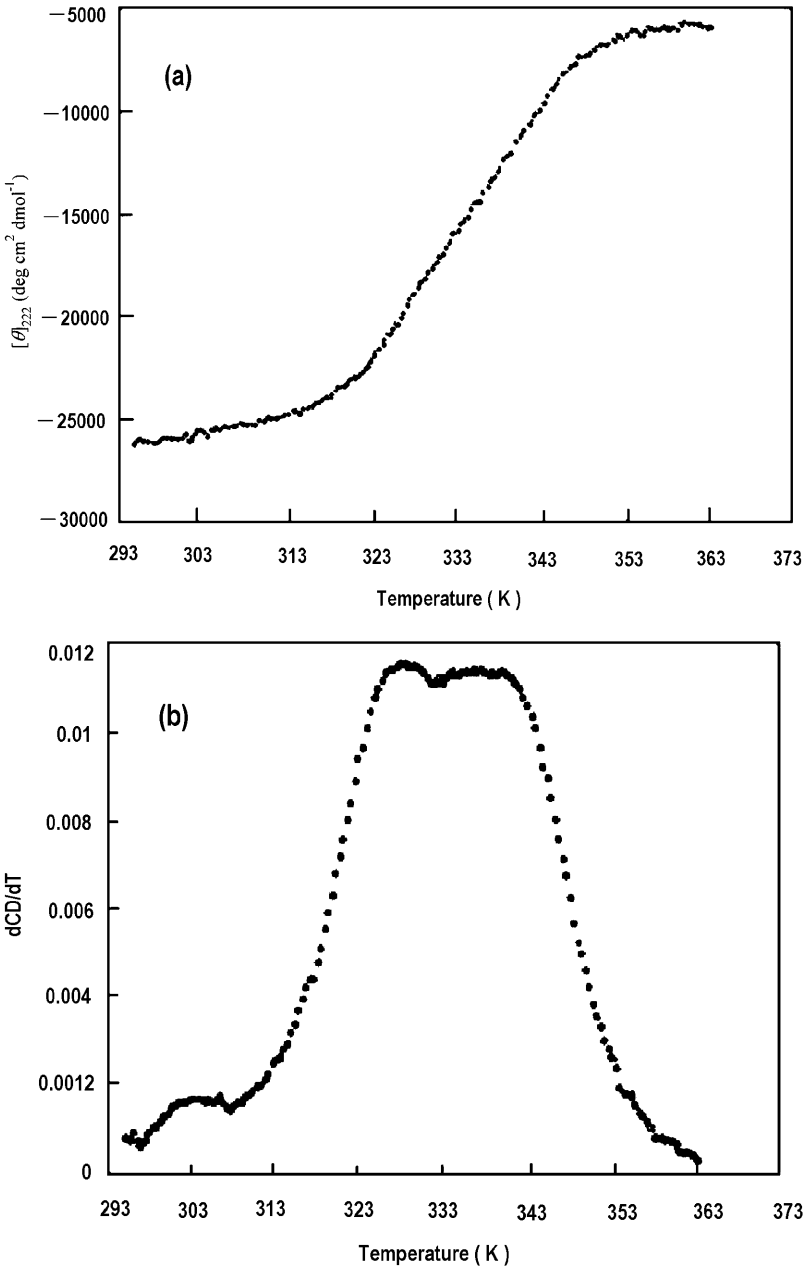

FIGURE 8 (*a*) Temperature dependence of the residue ellipticity, $[\theta_{222}]$, of gp57A at 222 nm in 50 mM sodium phosphate buffer, pH 8.0. (*b*) Derivative of the $[\theta_{222}]$ in *a*, with respective to temperature reveals two peaks corresponding approximately to the two T_m values in DSC, indicating that both transitions accompany a decrease in α-helicity.

data analyzed by global fitting with numerical solutions of the Lamm equation that finally yielded the unambiguous reaction scheme which is supported by DSC and stopped-flow CD. This approach makes use of the differential migration of the oligomeric species in the centrifugal field, which produces characteristic boundary shapes for different self-association schemes. It is worthwhile to note that the boundary shapes from fast and slow reversible systems are quite different, and no good fit can be expected from a Lamm equation model that assumes fast reversibility, if in fact the species are slow. An example of this has been published (Perugini et al., 2000). In that case, the reaction was slow, and the article shows how different the best-fit Lamm equation model with fast kinetics would be. However, we have shown by stopped-flow CD that the association reaction of gp57A is completed within 1 second, which is much faster than the duration of the experiment, i.e., on the order of an hour or longer.

Oligomeric states as defined in AUC analysis may not be identical with those of DSC analysis. In fact, the conformation of the monomeric state in the diluted solution at 20°C, for example, may well be different from the monomeric state at high temperature. This means that the involved intersubunit or interoligomeric interactions defined by the association constants, K_{1-3}, K_{3-6}, and K_{6-12}, have to be defined for each experimental condition for each methodol-

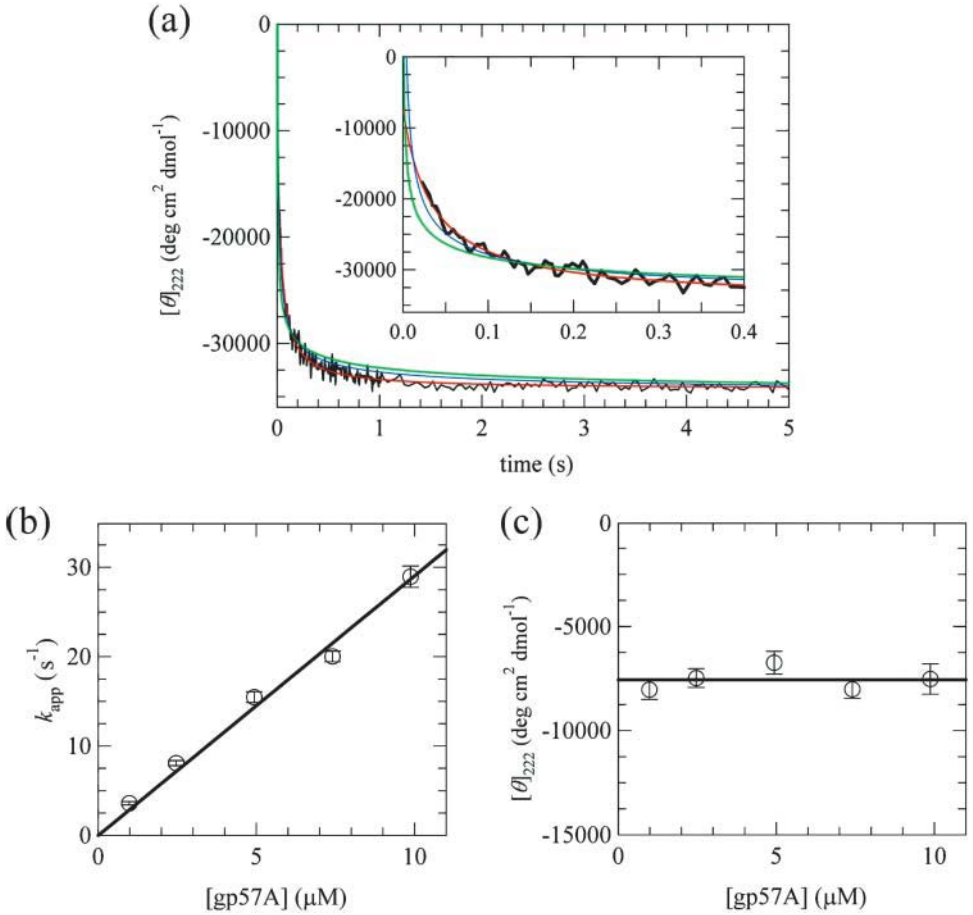

FIGURE 9 (*a*) A representative kinetic refolding curve of gp57A monitored by stopped-flow CD at 222 nm (*black line*). *Inset* shows the curve within 0.4 s of the refolding reaction. Protein concentration was 9.87 μM. The fitting curves assuming the bimolecular, trimolecular, and tetramolecular reactions (see Materials and Methods) are also shown by red, blue, and green lines, respectively. (*b*) Dependence of the apparent rate constant (k_{app}) on the protein concentration. The straight line is the best fit using the equation $k_{app} = 2[\text{gp57A}]k_f$ with $k_f = (1.45 \pm 0.04) \times 10^6\ M^{-1}\ s^{-1}$. (*c*) The ellipticity value at zero time of the refolding reaction plotted against the protein concentration. The straight line shows the average value of the data ($-7560 \pm 240°\ cm^2\ dmol^{-1}$).

ogy in a strict sense. However, the fact that the three distinct approaches gave rise to the same reaction scheme indicates that the intersubunit or oligomeric interactions such as 1_{mer}-1_{mer} interactions in 3_{mer}, 3_{mer}-3_{mer} interactions in 6_{mer}, or 6_{mer}-6_{mer} interactions in 12_{mer} are similar under the different conditions in the three approaches used in the present study, namely AUC, DSC, and stopped-flow CD. Although sedimentation equilibrium did not elucidate the association scheme unambiguously, now that the association scheme is known, we could compare the K_{3-6} and K_{6-12} as determined by sedimentation velocity experiments with those from sedimentation equilibrium. The latter gave the values for K_{3-6} and K_{6-12} as $(2.17 \pm 0.10) \times 10^4\ M^{-1}$ and $(2.63 \pm 0.10) \times 10^4\ M^{-1}$, respectively, which is, in fact, in agreement with the values obtained from sedimentation velocity—namely, $K_{3-6} = (3.4 \pm 0.6) \times 10^4\ M^{-1}$ and $K_{6-12} = (7.62 \pm 1.3) \times 10^3\ M^{-1}$, respectively.

Prediction of the structure of gp57A based on the amino acid sequence

Under the physiological or semiphysiological conditions, more than 90% of the primary structure assumes α-helix (Matsui et al., 1997). Several empirical rules have been reported concerning the number of helices to form coiled-coils. When the amino acid sequence of gp57A is arranged according to the helical wheel or heptad repeats (Mclachlan and Stewart, 1975), the *a*-positions are occupied by *IIASLV* and *d*-position by *LLTLLI*. The preference of specific amino acids at these core positions for dimeric and trimeric coiled-coils appears to be determined in terms of differences in packing geometry in these structures. The packing at *a*- and *d*-sites in trimers is more similar than in dimers (Wilson et al., 1981; Harbury et al., 1993, 1994; Delano and Brünger, 1994). According to earlier observations (Parry, 1982), a number of polar side chains occur at the *a*-positions more often than was expected by chance. In general, lysine (K) and arginine (R) are favored at the *a*-positions in dimers, but are absent in trimers. In addition, asparagines (N) are found three times more often at the *a*-sites of dimers than in the corresponding sites in trimers. In contrast, trimers or trimeric coiled-coil are enriched in glutamine (Q), serine (S), and threonine (T) residues at the *a*-sites and enrichment of polar side chains at position *d* is limited to preferences for serine (S) and threonine (T). In particular, experiments using synthetic peptides suggest that valine (V) at *a*-position specifies dimeric coiled-coils poorly (Harbury et al., 1993; Zhu et al., 1993). Also, packing in trimers is more permissive

than in dimers (Harbury et al., 1994). According to all these previous observations, the heptad structure in gp57A appears to favor trimers. This is in agreement with our conclusion that gp57A is in equilibrium among oligomeric species of 3_{mer}-6_{mer}-12_{mer}.

Plausible polypeptide arrangement and polarity

The next question is how the subunits or polypeptide chains are arranged in the trimeric and higher-order oligomeric coiled-coil of gp57A, especially in terms of polypeptide polarity. From the point of structural symmetry, it may be argued that the same polarity for all three α-helices may be favored. Also, in the above argument of heptad repeats, hydrophobic stabilization energy is assumed to provide the main driving force for the formation of coiled-coils from helical monomers and may even influence the stoichiometry and strand polarity of the coiled-coil. However, some other factors have to be considered for the preference of the polarity. It may be stabilized by other forces such as salt bridges or hydrogen bonds at the cost of introduction of asymmetry. There are nine excess negative over positive charges in gp57A, where the C-terminus, ^{73}DEAKDEE^{79}, is especially rich in negative charges. The *up-up-down* polarity of gp57A may provide electrostatic stabilization energy in the form of favorable interactions between dipole moments of antiparallel α-helical pairs (helices I and II; helices I and III). In fact, it was shown that a peptide, which was designed to form a double-stranded, parallel coiled-coil, turned out to be a triple-stranded α-helices which runs *up-up-down* (Lovejoy et al., 1993). It is, therefore, plausible that gp57A also assumes the triple-stranded α-helix.

Structure-function relation of gp57A

Gp57A functions as a molecular chaperone for the long and short tail fibers of bacteriophage T4. It has been shown that gp57A facilitates the formation of trimeric P12 in vitro as well as in vivo, where ATP is not required (Burda and Miller, 1999). A partial three-dimensional structure of the target protein, P12, has been solved by x-ray crystallography (van Raaij et al., 2001). It revealed a short three-stranded β-helix as well as β-spirals, which is similar to that of the adenovirus spike protein (van Raaij et al., 1999b). At present, nothing is known about the mode of interaction between gp57A and P12 upon folding of the former. Also, it is not possible to specify one particular species, but apparently, trimer or hexamer is biologically active as a molecular chaperone. Crystallization and structural determination of gp57A is underway.

We thank Dr. Allen P. Minton for his advice on the analysis of the data from sedimentation equilibrium.

This work was supported in part by a grant to F.A. from the Ministry of Education, Science, Sports and Culture of Japan, and from the National Project on Protein Structural and Functional Analyses.

REFERENCES

Arai, M., and K. Kuwajima. 1996. Rapid formation of a molten globule intermediate in refolding of α-lactalbumin. *Fold. Des.* 1:275–287.

Bishop, J. R., M. P. Conley, and W. B. Wood. 1974. Assembly and attachment of bacteriophage T4 tail fibers. *J. Supramol. Struct.* 2:196–201.

Burda, M. R., and S. Miller. 1999. Folding of coliphage T4 short tail fiber in vitro. Analysing the role of a bacteriophage-encoded chaperone. *Eur. J. Biochem.* 265:771–778.

Cox, D. J. 1969. Computer simulation of sedimentation in the ultracentrifuge. IV. Velocity sedimentation of self-associating solutes. *Arch. Biochem. Biophys.* 129:106–123.

Dam, J., and P. Schuck. 2003. Calculating sedimentation coefficient distributions by direct modeling of sedimentation velocity data. *Methods Enzymol.* In press.

Delano, W. L., and A. T. Brünger. 1994. Helix packing in the proteins: prediction and energetic analysis of dimeric, trimeric, and tetrameric GCN4 coiled coil structures. *Proteins Struct. Funct. Genet.* 20:105–123.

Dickson, R. C. 1973. Assembly of bacteriophage T4 tail fibers. IV. Subunit composition of tail fibers and fiber precursors. *J. Mol. Biol.* 79:633–647.

Harbury, P. B., T. Zhang, P. S. Kim, and T. Albert. 1993. A switch between two-, three-, and four- stranded coiled coils in GCN4 leucine zipper mutants. *Science.* 262:1401–1407.

Harbury, P. B., P. S. Kim, and T. Albert. 1994. Crystal structure of an isoleucine-zipper trimer. *Nature.* 371:80–83.

Hashemolhosseini, S., Y. Stierhof, I. Hindennach, and U. Henning. 1996. Characterization of the helper proteins for the assembly of tail fibers of coliphages T4 and λ. *J. Bacteriol.* 178:6258–6265.

Henning, U., and K. Jann. 1979. Two-component nature of bacteriophage T4 receptor activity in *Escherichia coli* K-12. *J. Bacteriol.* 137:664–666.

Kells, S. S., and R. Haselkorn. 1974. Bacteriophage T4 short tail fibers are the product of gene 12. *J. Mol. Biol.* 83:473–485.

Kidokoro, S., H. Ueaira, and A. Wada. 1988. Determination of thermodynamic functions from scanning calorimetry data. II. For the system that includes self-dissociation/association process. *Biopolymers.* 27:271–290.

King, J., and U. K. Laemmli. 1971. Polypeptides of the tail fibers of bacteriophage T4. *J. Mol. Biol.* 62:465–477.

Kuwajima, K., H. Yamaya, S. Miwa, S. Sugai, and T. Nagamura. 1987. Rapid formation of secondary structure framework in protein folding studied by stopped-flow circular dichroism. *FEBS Lett.* 221:115–118.

Lamm, O. 1929. Die differentialgleichung der ultrazentrifugation. *Ark. Mat. Astr. Fys.* 21B:1–4.

Lovejoy, B., S. Choe, D. Cascio, D. K. McRorie, W. F. DeGrado, and D. Eisenberg. 1993. Crystal structure of a synthetic triple-stranded α-helical bundle. *Science.* 259:1288–1293.

Mason, W. S., and R. Haselkorn. 1972. Product of T4 gene 12. *J. Mol. Biol.* 66:445–469.

Matsui, T., B. Griniuviené, E. Goldberg, A. Tsugita, N. Tanaka, and F. Arisaka. 1997. Isolation and characterization of a molecular chaperone, gp57A, of bacteriophage T4. *J. Bacteriol.* 179:1846–1851.

Mclachlan, A. D., and M. Stewart. 1975. Tropomyosin coiled-coil interactions: evidence for an unstaggered structure. *J. Mol. Biol.* 98: 293–304.

Milla, M. E., and R. T. Sauer. 1994. P22 Arc repressor: folding kinetics of a single-domain, dimeric protein. *Biochemistry.* 33:1125–1133.

Mutoh, N., H. Furukawa, and S. Mizushima. 1978. Role of lipopolysaccharide and outer membrane protein of *Escherichia coli* K-12 in the receptor activity for bacteriophage T4. *J. Bacteriol.* 136:6913–6919.

Nakagawa, T., and T. Oyanagi. 1980. Program system SALS for nonlinear least-squares fitting in experimental sciences. *In* Recent Developments in Statistical Inference and Data Analysis. K. Matusita, editor. North Holland Publishing, Amsterdam, The Netherlands. 221–225.

Parry, D. A. D. 1982. Coiled coils in α-helix containing proteins: analysis of the residue types within the heptad repeat and the use of these data in the prediction of coiled coils in other proteins. *Biosci. Rep.* 2:1017–1024.

Perugini, M. A., P. Schuck, and G. J. Howlett. 2000. Self-association of human apolipoprotein E3 and E4 in the presence and absence of phospholipids. *J. Biol. Chem.* 275:36758–36765.

Prehm, P., B. Jann, K. Jann, G. Schmidt, and S. Stirm. 1976a. On a bacteriophage T3 and T4 receptor region within the cell wall lipopolysaccharide of *E. coli* B. *J. Mol. Biol.* 101:277–281.

Provencher, S. W., and J. Glockner. 1981. Estimation of globular protein secondary structure from circular dichroism. *Biochemistry.* 20:33–37.

Revel, H. R., R. Hermann, and J. R. Bishop. 1976. Genetic analysis of T4 tail fiber assembly. II. Bacterial host mutants that allow bypass pf T4 gene 57 function. *Virology.* 72:255–265.

Riede, I. 1987. Receptor specificity of the short tail fibers (gp12) of T-even type *Escherichia coli* phages. *Mol. Gen. Genet.* 206:110–115.

Rivas, G., J. A. Fernandez, and A. P. Minton. 1999. Direct observation of the self-association of dilute proteins in the presence of inert macromolecules at high concentration via tracer sedimentation equilibrium: theory, experiment, and biological significance. *Biochemistry.* 38:9379–9388.

Schuck, P. 2000. Size distribution analysis of macromolecules by sedimentation velocity ultracentrifugation and Lamm equation modeling. *Biophys. J.* 78:1606–1619.

Schuck, P., M. A. Perugini, N. R. Gonzales, G. J. Howlett, and D. Schubert. 2002. Size distribution analysis of proteins by analytical ultracentrifugation: strategies and application to model systems. *Biophys. J.* 82:1096–1111.

Schuck, P. 2003. On the analysis of protein self-association by sedimentation velocity analytical ultracentrifugation. *Anal. Biochem.* In press.

Schuck, P. 1998. Sedimentation analysis of noninteracting and self-associating solutes using numerical solutions to the Lamm equation. *Biophys. J.* 75:1503–1512.

Schuck, P., and B. Delemer. 1999. Direct sedimentation analysis of interference optical data in analytical ultracentrifugation. *Biophys. J.* 76: 2288–2296.

Simon, L. D., and T. F. Anderson. 1967. The infection of *Escherichia coli* by T2 and T4 bacteriophages as seen in the electron microscope I. Attachment and penetration. *Virology.* 32:279–297.

Steinfeld, J. I., J. S. Francisco, and W. L. Hase. 1989. Chemical Kinetics and Dynamics. Prentice-Hall, Englewood Cliffs, NJ.

Studier, F. W., and B. A. Moffatt. 1986. Use of bacteriophage T7 RNA polymerase to direct selective high-level expression of cloned genes. *J. Mol. Biol.* 189:113–130.

van Raaij, M. J., G. Schoehn, M. R. Burda, and S. Miller. 2001. Crystal structure of a heat and protease-stable part of the bacteriophage T4 short tail fiber. *J. Mol. Biol.* 314:1137–1146.

van Raaij, M. J., A. Mitraki, G. Lavigne, and S. Cusack. 1999b. A triple β-spiral in the adenovirus fiber shaft reveals a new structural motif for a fibrous protein. *Nature.* 401:1049–1055.

Wilson, I. A., J. J. Skehel, and D. C. Wiley. 1981. Structure of the haemagglutinin membrane glycoprotein of influenza virus. *Nature (Lond).* 289:366–373.

Wood, W. B., and J. R. Bishop. 1973. Bacteriophage T4 tail fibers: structure and assembly of a viral organelle. *In* Virus Research. C. F. Fox, and W. F. Robinson, editors. Academic Press, New York. 303–324.

Wood, W. B., F. A. Eiserling, and R. A. Crowther. 1994. Long tail fibers: genes, proteins, structure, and assembly. *In* Molecular Biology of Bacteriophage T4. J. D. Karam, editor. American Society for Microbiology, Washington, DC. 282–290.

Zhu, B. Y., N. E. Zhou, C. M. Kay, and R. S. Hodges. 1993. Packing and hydrophobicity effects on protein folding and stability of two-stranded α-helical coiled coils/leucine zippers. *Protein Sci.* 2:383–394.